# COMPUTATIONAL MODELING OF HEAT TRANSFER AND FLOW SEPARATION IN SUPERSONIC COOLED NOZZLES: PARAMETRIC STUDY

**BENSAYAH Khaled[1,2,*], KAMRI Khadidja[1]**

[1]Interprofessional Complex Research in Aerothermochemistry CORIA UMR 6614 CNRS, INSA of Rouen, France
[2]Laboratory of Mechanic, department of mechanical engineering, University of Laghouat, Algeria.
[*] Corresponding author; Email: k.bensayah@lagh-univ.dz

*Flow separation is necessary for the construction of a rocket engine nozzle. Regenerative cooling is one of the most significant criteria for the safety of wall nozzles because of the high temperature and pressure in the thrust chamber. A review of a comprehensive numerical investigation of the boundary layer separation and heat transfer in a 30°−15° cooled nozzle is presented. The accuracy of the SST-V turbulence model in this study was numerically investigated. For this purpose and for a wide range of chamber conditions, the effects of various parameters, such as wall temperature, turbulent Prandtl number, and constant specific heat ratio vary from 1.31 to 1.4 for constant fluid properties for $N_2O$, $CH_4$, $Cl_2$, and air, respectively. The variable specific heat ratio ranged from 1.39 to 1.66 for variable fluid properties for air, $CH_4$, $O_2$ and Helium, respectively, and we investigated how various parameters impact the position of flow separation and local wall heat transfer.*

Keywords: separation location, heat transfer, Compressible flow, Regenerative nozzle cooling, High temperature flows

## 1. Introduction

The behavior of fluid mechanics and heat transfer in an accelerated turbulent flow differs significantly from that in nonaccelerating cases. Supersonic nozzle flows are crucial for the design, development, and fundamental research purposes. Consequently, numerous studies have been conducted worldwide to investigate and gain a better understanding of heat transfer phenomena in rocket nozzles, which are strongly influenced by a range of parameters, including combustion dynamics, injection schemes, and turbulence levels. The heat transfer in nozzles occurs in the presence of a large pressure gradient and at very high stagnation temperatures, which is manifested by the presence of two components: a convective component to which another so-called radiation is superimposed.

Initially, most of the studies and investigations were mainly focused on the study of the convective phenomenon in pipes and conical nozzles with a low angle of divergence and low pressure and stagnation temperature [1], [2], [3] and [4].

Back et al. [5] experimentally investigated the effects of several parameters, such as stagnation pressure and temperature, as well as the thickness of the boundary layer on convective heat transfer. They found that the coefficient of heat transfer increased with increasing stagnation pressure in the case of a turbulent boundary layer. The effects of stagnation temperature, for its part, are no longer clear. Back et al. [5] also noted that a thinner boundary layer at the inlet led to an elevated heat transfer coefficient.

The same remarks were reported by Leccese et al. [6], who aimed to compare two types of transfer (convective and radiative) in a thrust chamber. As a result, the authors found that the heat flux decreased along the chamber because of the thickening of the boundary layer, which prevented the convective contribution, while the radiative contribution remained constant. The authors also investigated the effects of a combustion mixture of (O/CH4) and (O/H).

They found that the resulting chemical elements only affected radiation. However, convection only depends on the thermal conductivity of the mixture, and consequently, the heat transfer in the case of (O/H) was more important. The same remarks on the effect of increasing the chamber pressure reported by Back et al. (1963) were made by Leccese et al. [6]. Concerning the effects of wall temperature, Leccese et al. [6] reported that the convective flow decreases by increasing the temperature of walls because of the small difference between the flow temperature and the wall temperature.

In their experimental investigation, Arnold et al. [7] examined the parameters affecting the efficiency of cooling film in a model high-pressure combustion chamber. They specifically focused on studying the impact of film blowing and the ratio between injection speed and gas speed. The study revealed that increasing film blowing led to improved efficiency, while an increase in injection speed ratio and Reynolds number of the slot contributed to enhancing film efficiency.

Miranda et al. [8] analyzed how flow films affect heat transfer in thrust chambers. Their study encompassed various characteristics such as flow and composition effects. Overall, the results indicated that hydrogen was more effective than an (O/f) mixture at reducing heat transferred to walls for a fixed wall temperature. However, there are instances where using an (O/f) mixture is necessary due to potential over-cooling caused by hydrogen.

Other effects have been investigated, such as the injection angle and height of the slots [9], as well as chemical reactions [10]. The effects of altitude were investigated by Kim et al. [11], who reported that the transfer of heat decreases with increasing altitude, which is an obvious consequence of a decrease in the density of air. In his study, which aimed to model the heat transfer in a thrust chamber, Daimon et al. [12] specified the importance of considering the elements resulting from combustion as well as the interaction between the flames and the walls of the thrust chamber. Similar results were confirmed by Frank and Pfitzner [13].

Although many authors have studied this subject, there has not yet been a thorough analysis of the phenomenon as a whole nor have appropriate methodologies been developed. We explored the heat transfer characteristics associated with the turbulent flow of hot air through a converging- diverging nozzle to fill some of the gaps statistically. We started this numerical study to enhance our understanding of how various parameters affect the steady flow of fluid through nozzles and to explain the effect of some important parameters such as the turbulent Prandtl number, wall temperature, and specific heat ratio (γ), on the heat transfer distribution of the wall, and on the static pressure of the wall (separation position) for adiabatic and isothermal walls.

## 2. Turbulence modeling and numerical method

### 2.1 Turbulence modeling

To prevent computational problems related to employing the accurate source term of turbulent kinetic energy k. The variety of the Shear Stress Transport (SST), knowing by the combination of the advantages of the two models $k-\epsilon$ and $k-\omega$, called SST-V is used. The term responsible for producing k in this case is described by the local measure of the vorticity [16,17]. A reliable estimate of the production of the source term can be obtained from this formulation (see eq.2) in the boundary layer [6].

$$\tau_{ij} = \mu_t \left( \frac{\partial U_i}{\partial x_j} + \frac{\partial U_i}{\partial x_i} - \frac{2}{3} \frac{\partial U_k}{\partial x_k} \delta_{ij} \right) - \frac{2}{3} \rho k \delta_{ij} \tag{1}$$

$$\tau_{ij} \frac{\partial U_i}{\partial x_j} = \mu_t \Omega^2 - \frac{2}{3} \rho k \delta_{ij} \frac{\partial U_i}{\partial x_j} \tag{2}$$

The model in fact employs two extra transport equations to characterize the turbulence:

$$\frac{D}{Dt}(\rho k) = \tau_{ij} \frac{\partial U_i}{\partial x_j} - \beta^* \rho \omega k + \frac{\partial}{\partial x_j} \left( (\mu + \sigma_k \mu_t) \frac{\partial k}{\partial x_j} \right) \tag{3}$$

$$\frac{D}{Dt}(\rho \omega) = \frac{\gamma \rho}{\mu_t} \tau_{ij} \frac{\partial U_i}{\partial x_j} - \beta \rho \omega^2 + \frac{\partial}{\partial x_j} \left[ (\mu + \sigma_{\omega_1} \mu_t) \frac{\partial \omega}{\partial x_j} \right] + 2\rho(1 - F_1) \sigma_{\omega 2} \frac{1}{\omega} \frac{\partial k}{\partial x_j} \frac{\partial \omega}{\partial x_j} \tag{4}$$

Where $D/Dt = \partial/\partial t + u_j \partial/\partial x_j$ is the Lagrangian derivative. The blending function $F_1$ is given by the following:

$$F_1 = \tanh \left\{ \left( min \left( max \left( \frac{\sqrt{k}}{0.09 \omega y}, \frac{500 \mu}{\rho \omega y^2} \right), \frac{4 \rho \sigma_{\omega 2} k}{C D_{k\omega} y^2} \right) \right)^4 \right\} \tag{5}$$

Here, the term $CD_{k\omega}$ denotes a cross-diffusion included in Eq. (4). The eddy viscosity is taken as following: $\mu_t = \rho a_1 k / \max(a_1\omega, \Omega F_2)$, where $F_2$ is a function, used only on the boundary layer, given by:

$$F_2 = \tanh\left(\left(max\left(\frac{2\sqrt{k}}{0.09\omega y}, \frac{500\nu}{y^2\omega}\right)\right)^2\right)$$

**2.2 Numerical method**

The set of equations is presented in a conservative format, segregating the contributions from viscous and non-viscous sources. The terms $S_0$, are processed distinctly.

$$\frac{\partial U}{\partial t} + \frac{\partial F(U)}{\partial x} + \frac{\partial G(U)}{\partial y} = \frac{\partial F_v(U)}{\partial x} + \frac{\partial G_v(U)}{\partial y} + S_0(U) \tag{6}$$

here U represents the vector of conservative variables,

$$U = \begin{pmatrix} \bar{\rho} \\ \bar{\rho}\tilde{u} \\ \bar{\rho}\tilde{v} \\ \bar{\rho}\tilde{E} \\ \bar{\rho}k \\ \bar{\rho}\omega \end{pmatrix}, \quad S_0 = \begin{pmatrix} 0 \\ 0 \\ 0 \\ 0 \\ H_k \\ H_\omega \end{pmatrix} \tag{7}$$

In this context, F and G denote the inviscid flux, while Fν, Gν refer to the viscous vectors,

$$F = \begin{pmatrix} \bar{\rho}\tilde{u} \\ \bar{\rho}\tilde{u}\tilde{u} + p^* \\ \bar{\rho}\tilde{u}\tilde{u} \\ \left(\bar{\rho}\tilde{E} + p^*\right)\tilde{\rho} \\ \bar{\rho}\tilde{u}k \\ \bar{\rho}\tilde{u}\omega \end{pmatrix}, \qquad G = \begin{pmatrix} \bar{\rho}\tilde{v} \\ \bar{\rho}\tilde{v}\tilde{u} \\ \bar{\rho}\tilde{v}\tilde{v} + p^* \\ \left(\bar{\rho}\tilde{E} + p^*\right)\tilde{v} \\ \bar{\rho}\tilde{v}k \\ \bar{\rho}\tilde{v}\omega \end{pmatrix} \tag{8}$$

Here, $\bar{\rho}$ denotes the density, x and y components of fluid velocity are $\tilde{u}$ and $\tilde{v}$, $\widetilde{E}$ is the total energy, and p is static pressure which is derived from the equation of state of perfect gas.

$$p = (\gamma - 1)\bar{\rho}\left(\tilde{E} - \frac{(\tilde{u}^2 + \tilde{v}^2)}{2} - k\right) \tag{9}$$

Here are the expressions for the viscous fluxes, $F_\nu$ and $G_\nu$

$$F_v = \begin{pmatrix} 0 \\ \tilde{\sigma}_{xx} \\ \tilde{\sigma}_{xy} \\ \tilde{\sigma}_{xx}\tilde{u} + \tilde{\sigma}_{xy}\tilde{v} - \bar{q}_x \\ \tilde{\sigma}_{kx} \\ \tilde{\sigma}_{\omega x} \end{pmatrix}, \qquad G_v = \begin{pmatrix} 0 \\ \tilde{\sigma}_{xx} \\ \tilde{\sigma}_{yy} \\ \tilde{\sigma}_{xy}\tilde{u} + \tilde{\sigma}_{yy}\tilde{v} - \bar{q}_y \\ \tilde{\sigma}_{ky} \\ \tilde{\sigma}_{\omega y} \end{pmatrix} \tag{10}$$

Here $\tilde{\sigma}$ denotes the stress-tensor, and $\bar{q}$ represents the vector of heat flux.
As for the numerical method, the equations of Navier-Stokes are solved using a finite volume predictor-corrector on a computational domain defined by variables ζ and η, which correspond to the transformed coordinates of the physical domain.

MacCormack's [18] explicit-implicit approach is used to solve the new system of equations. In terms of space and time, this method is second-order precise. Steger and Warming [19] modified the fundamental discretization method for convective fluxes in order to consider the physical characteristics of how information spreads. In shock zones, the flux splitting is reduced to first order. In both the ζ and η directional sweeps, the integration of the axisymmetric source terms takes place at the center of every control volume, while the viscous terms are centered as well.Explicit discretization is merged with an numerical implicit approximation that doesn't have any limitation of stability to arrive at a steady-state solution with the fewest number of iterations. In the η direction, to solve the block penta diagonal system, a generalized Thomas method with LU decomposition is employed, a line Gauss-Seidel relaxation technique is then used in the ζ direction. The method is iterative because the diagonally dominating system, a convergent steady solution can be produced in a relatively small number of time steps, each of which includes a backward-forward double sweep in the flow direction. Unbounded time step values can possibly be used with this technique. C.F.L greater than 15 [20] have been used in numerical calculations. In this paper, we focus on presenting the results of the present study. However, for a detailed explanation of the numerical method used and the equations involved, we refer to the reference [21].

## 3. Findings and discussion

### 3.1 Boundary conditions and model validation

The study utilized a conical nozzle identical to those in Bensayah et al. [22,23] and Cuffel et al. [29]. Prescribed total pressure and total temperature were applied at the inlet, with axisymmetric conditions maintained along the nozzle symmetry line. Initially, the walls were considered adiabatic for model validation, with subsequent modifications to wall conditions based on the specific case being studied. Figure (1.a) shows the axial distribution of computed and measured [29] static pressure at various radial locations, demonstrating a significant radial variation in static pressure with a gradient that closely mirrors the axial static pressure gradient. Figure (1.b) shows that gas expands faster along the wall than the centerline, likely due to compressive turning of the flow, which is associated with static-pressure increase behind the tangent between the throat circular arc and the conical diverging portion in figure (1.a). Flow overturning near the wall is observed due to the flow's ability to maintain high angular motion in the small curvature radius region near the throat. Consequently, the flow lines close to the wall slope towards the conical wall downstream. Mach number contours indicate the commencement of shock production associated with compressive twisting of the flow, with a weak oblique shock wave originating and propagating downstream, intersecting the centerline at x = 8 cm.

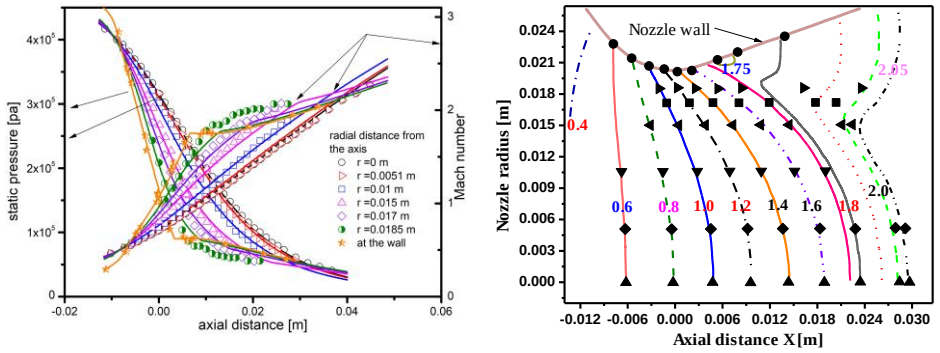


(a) (b)

Fig. 1. Validation of the computed results with experimental data [29] in the transonic region: (a) static pressure and Mach number, (b) Mach contours.

**Table 1**. Different test cases

| Case N° | Stagnation temperature | Stagnation pressure |
|---|---|---|
| Case 1 | $T_0 = 843.33$ K | $P_0 = 5.18$bar |
| Case2 | $T_0 = 572.22$ K | $P_0 = 17.49$bar |
| Case3 | $T_0 = 835.00$ K | $P_0 = 3.08$bar |

### 3.2 Effects of specific heat ratio on separation and static wall pressure

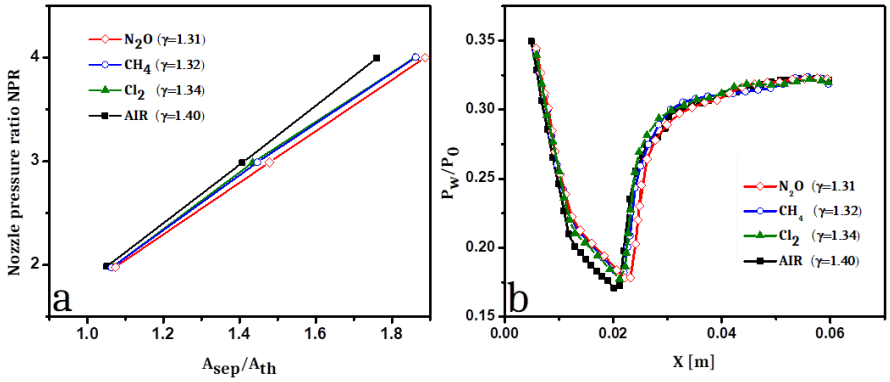


Fig. 2. Effect of $\gamma$ on (a) the location of separation, (b) the distribution of wall static pressure.

This section aims to investigate the impact of specific heat ratio (γ) on separation position in the nozzle, as presented in Figure 2 based on the reference by Back et al. [5]. However, isolating the effect of specific heat ratio alone is challenging due to other variables such as specific heat and molar mass being involved.

To address this challenge, a cold temperature of 300K is used to eliminate the temperature dependence of specific heat. Additionally, a power law relationship ($\mu/\mu_0 = (T/T0)^m$) is employed to mitigate viscosity effects. In Figure 2a, it can be observed that increasing the specific heat ratio results in a downstream shift in separation location. Nevertheless, drawing firm conclusions solely based on this observation remains insufficient due to the involvement of both specific heat and specific heat ratio.

To gain further insights into this matter, a comparison between air and $N_2O$ gas is conducted since they have identical values for specific heat. Similar observations are made when comparing these gases, particularly with an increase in stagnation pressure. Moreover, Figure 2b demonstrates that decreasing the value of specific heat ratio leads to an increase in wall pressure, detailed information regarding the physical properties of gases is provided in Table 2.

**Table 2** Different gases physical properties

| Gas | $m$ | $R[m^2s^{-2}K^{-1}]$ | $C_p[J\mathrm{Kg}^{-1}K^{-1}]$ | $\gamma$ |
|---|---|---|---|---|
| $N_2O$ | 0.89 | 189 | 798.6 | 1.31 |
| $CH_4$ | 0.87 | 518 | 2136.7 | 1.32 |
| $Cl_2$ | 1 | 117 | 461.1 | 1.34 |
| Air | 0.67 | 287 | 1004.5 | 1.4 |

The effect of γ on the position of the separation point is studied with gases that have γ ranging from 1.3 for ch4 to 1.66 for helium gas. The physical properties of the gases are variable (cp, γ, μ, λ).

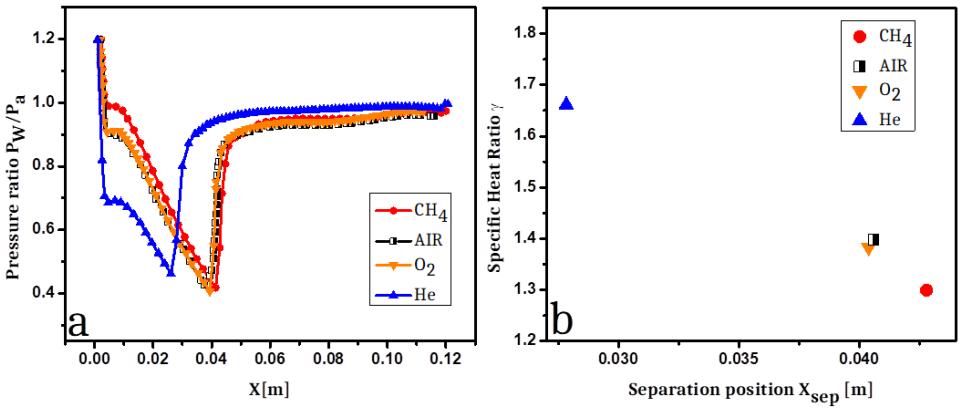


Fig. 3. (a) wall static pressure distribution, (b) effect of gas nature on the position of separation

The analysis of figure (3.a) well zoomed in, shows that the position of the boundary layer separation point moves upstream for increase $\gamma$, in other words, this position moves downstream for more $\gamma$ decreases. For more detail, the exact detachment point positions are shown in figure (3.b), the difference is significant between helium and $CH_4$ of about of 35%. These results show that the real physical quantities of $C_p$, $\gamma$, $\mu$ and the conductivity $\lambda$, have an important effect on the calculation of the good behavior of the dynamic and thermal boundary layer.

### 3.3 Effects of the wall temperature on wall pressure

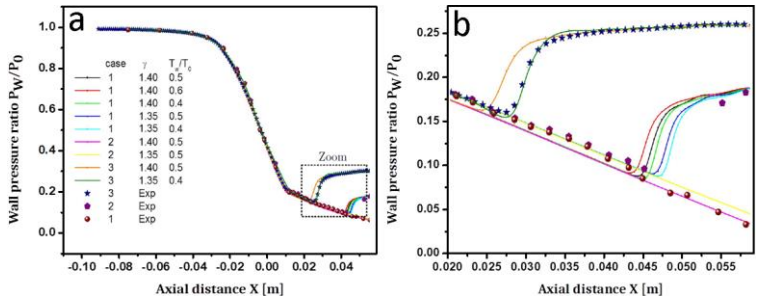


Fig. 4. (a) wall static pressure distribution, (b) Zoom on the separation region, Exp [5]

Figure 4a shows the normalized static wall pressure across the nozzle for various parameters, including chamber pressure and temperature ($P_0$, $T_0$), the ratio of specific heats $\gamma$, and wall temperature $T_W$. The turbulence model is validated against experimental data from Back et al. [5]. Figure 4b is a zoomed-in view of the separation region, highlighting the impact of the aforementioned parameters on both the wall pressure and separation points. The study also investigates the effect of wall temperature by considering three values ($Tw/T_0$ = 0.4, 0.5, and 0.6) corresponding to the experiment conducted by Back et al. [5].

The study shows that increasing the $T_W$ leads to an upstream shift in the separation point. However, when the Tw wall temperature is too high ($Tw/T_0$ = 0.6), the separation point differs from the experimental result, likely because the temperature used in the simulation is higher than the experimental value of $Tw/T_0$ = 0.42 in the supersonic and near-separation regions. The impact of wall temperature on separation is still not clear in the literature, although some studies suggest that cold walls may result in wider separation due to a larger wall Mach number at the initial separation point. The present findings are consistent with the experimental results reported in [24] and differ from those in [25]. The results of Schmucker [25] contradict theories about the effect of wall temperature on separation, as a cooler wall is expected to result in a lower separation pressure ratio.

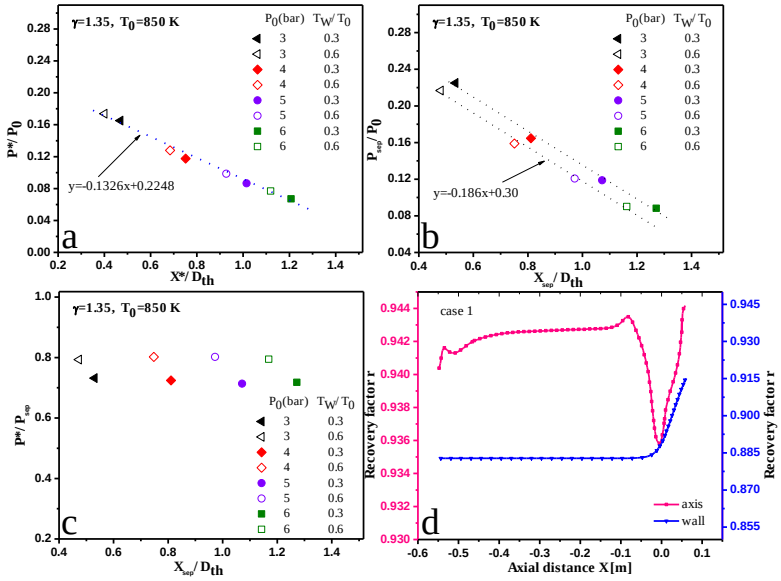


Fig. 5. (a) Different pressure distributions: (a) pressure at the initial point of the interaction region, (b) separation pressure versusthe Dimensionless separation position, (c) pressure at the initial point of the interaction region versus the Dimensionless separation position, (d) the recovery factor

Figures (5.a), (5.b) and (5.c) show the same tendency of figure (4.b). An increase in the stagnation pressure leads to downstream displacement of the separation location. For identical chamber pressure, the separation position moves downstream when decreasing the wall temperature.

It can be seen that the findings with $\gamma = 1.35$ are significantly better; this value is in agreement with Vieser et al. [16] and Tong and Luke [17].

### 3.4 Effects of turbulent Prandlt number on wall heat transfer coefficient

Wall heat transfer coefficient $h$, given by $h = q_w/(T_{aw} - T_w)$, is investigate in this part of the paper For this purpose, Walls are considered to be adiabatic with a temperature $T_{aw}$ calculated as following:

$$\frac{T_{aw}}{T_0} = \frac{1 + (r/2)(\gamma - 1)M^2}{1 + (0.5)(\gamma - 1)M^2}$$

Where $r$ is the temperature recovery factor. Figure (5.d) shows the recovery factor variation along the nozzle. As cited by [26], the recovery factor is dependent on a number of variables. near the wall, the recovery factor decreases upstream the nozzle throatand increases immediately downstream the throat, this behavior seems to be opposite to that of the heat transfer, as well as to the thermal conductivity and the specific heat. On the axis, this behavior is opposite due to the temperature decrease outside the boundary layer. The describedbehavior can be explained by a more pronounced relaxation outside of the boundary layer. The recovery factor is next taken as $r = 0.89$, the value was calculated using $r = Pr^{1/3}$, for the hole simulation. The axial evolution of the wall heat transfer coefficient $h$ for different Prandlt number value is presented in figure (6.a). The effect of the turbulent seems to be clear especially in the subsonic region where increasing the $Pr_t$ number results in more important values of wall heat transfer coefficient $h$.

The advanced remarks confirmed the ascertainments of Xiao et al [14] and those of Sommer et al [27,15]. To shed more lights on the effect of the Prandlt number, the calculations are carried out using a variable $Pr_t$ since a constant turbulent Prandlt number value no longer appropriate for the entire flow. The turbulent Prandlt number is now defined as [28]:

$$P_{rt} = 0.67\frac{1+0.67f}{1+0.5f}(1+0.167f)$$

With

$$\begin{cases} f = min(R_t/3.72R_k, 1) \\ R_t = k^2/\epsilon\mu, R_k = \sqrt{k}yl/\mu \end{cases}$$

Figure (8.a) shows the calculated turbulent Prandlt number while figure (8.b) displays the computed wall heat transfer coefficient h in both cases; using a fixed prandlt number value and using a variable value of the Prandlt number. Its clear that the subsonic region is less affected since just a small decrease of the Prandlt number can be observed in the boundary layer close to the wall. The major differences can be seen downstream, especially before the throat, where a steep decrease in the Prandlt number can be observed far-away from the wall. These differences start to vanish when moving downstream toward the divergent.

As shown before, the heat transfer coefficient h is a function of the three parameters: Adiabatic wall temperature, wall temperature and the heat transfer flux throw the wall.

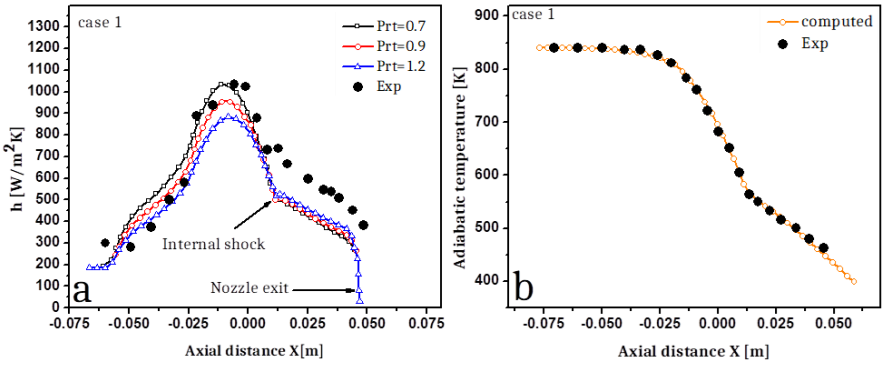


Fig. 6. (a) Heat transfer coefficient with different Prt values, (b) comparison of calculated adiabatic wall temperature against experimental data [5]

Figure (6.b) demonstrates strong agreement between the adiabatic wall temperature obtained from the computations and the experimental results presented by Back et al. (1963). This close correspondence between the two sets of data enables us to deduce that the variations in the heat transfer coefficient observed earlier can be attributed to differences in the wall temperature distribution and computed wall heat transfer.

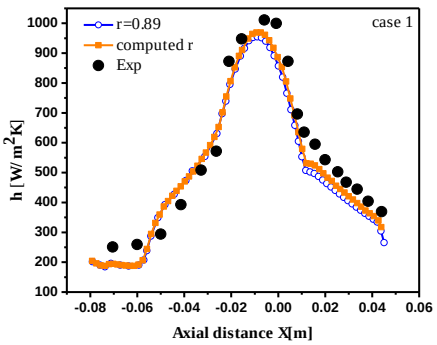


Fig. 7. Heat transfer coefficient with different recovery factor configurations, Exp [5]

The wall temperature for this case (case 1, see Table 1) is found to be varying over a range exceeding 100k, particularly in the critical throat region. Using the experimental wall temperature will correct the situation by lowering the observed heat transfer maximum by almost 30%.

Figure 7 shows the heat transfer coefficient distribution along the nozzle for case 1 using both calculated and prescribed recovery factor. Heat transfer coefficient exhibits a good agreement with experiment data [5] mainly in the subsonic region.

After that, the difference becomes important downstream the internal shock. It is worth to remind that the differences here come from several sources. First, it comes from the fixed wall temperature together with the computed wall heat transfer flux which involves itself many parameters among them; the specific heat which changes along the flow field. To the previous reasons, the accuracy of the turbulence model, when calculating the turbulent boundary layer growth in supersonic region, is added. In fact, the boundary layer growth in this region is strongly influenced by the internal shock wave shown in figure 7.

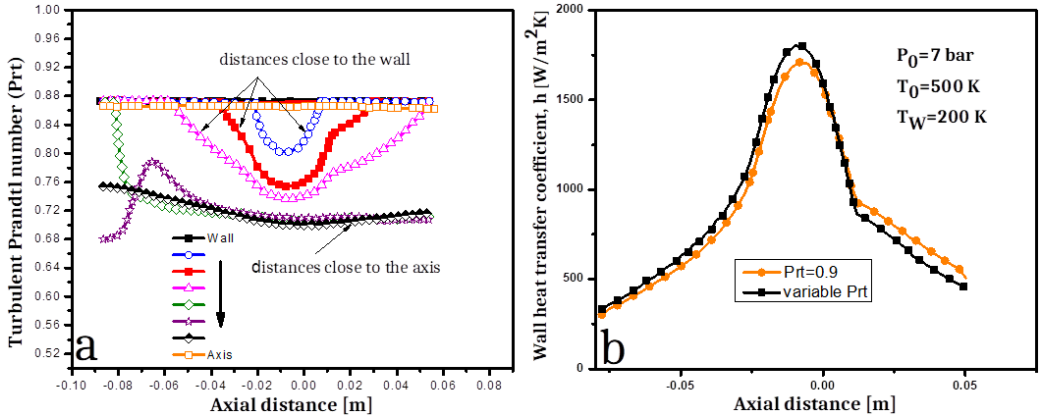


Fig. 8. (a) distribution of variable $Pr_t$, (b) Effect of $Pr_t$ variation on the distribution of wall heat flux

### 3.5 Effects of wall temperature and specific heat ratio on wall heat transfer coefficient

Decreasing the wall temperature leads the wall heat flux to slightly increase as shown in figure (9.a). This behavior can be ascribed to the dependence of the heat transfer flux on the difference of temperature between the wall temperature and the core flow temperature. The effects of specific heat ratio on the other hand, shown in figure (9.b), reveal an increase in the rate of the heat transfer flux as an answer of the immediate decrease of the specific heat ratio.

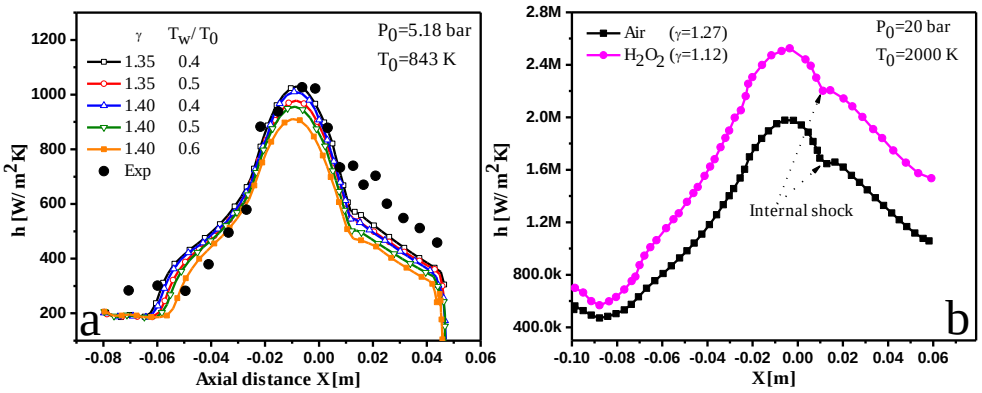


Fig. 9. effect of (a) the wall temperature and (b) specific heat ratio (gas nature), on the distribution of wall heat transfer coefficient, Exp [5]

### 3.6 Effects of chamber pressure and temperature

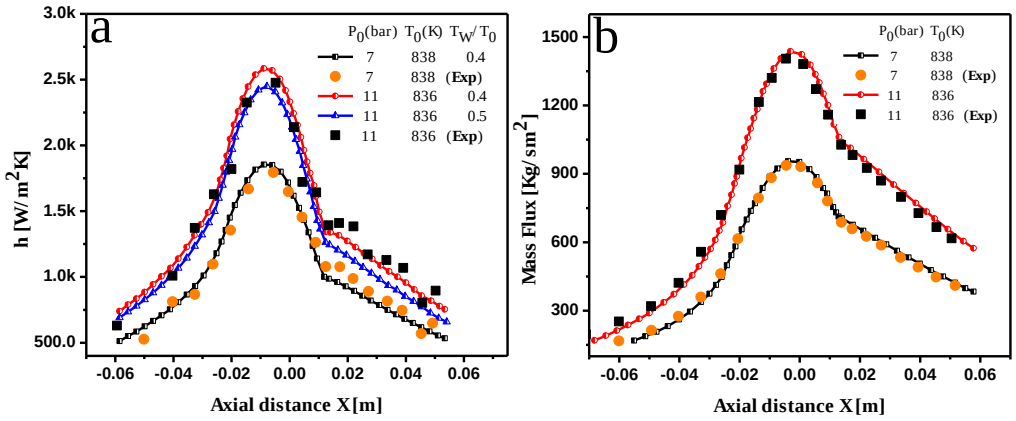


Fig. 10. (a) effect of the stagnation pressure on the wall heat coefficient, (b) effect of stagnation pressure on the mass flux distributionat the edge of the boundary layer, Exp [5]

As reported by many researchers [6] [10], the heat transfer coefficient increases by increasing the chamber pressure figure (10.a). In fact, the coefficient of heat transfer increases due to the increase in mass flow (figure (10.b)) resulting from the increase of the total pressure $P_0$. As shown in figure (10.b), the maximum value of the heat transfer agrees very well with the one of the mass flow, this position is situated just upstream of the throat. The effect of increasing the chamber temperature are found to be less clear for low chamber pressure. Worth to be reported, the heat transfer coefficient is found to be decreasing when increasing temperature.

## 4. Conclusions

This computational work examined the effects of various effects significant parameters on both thermal and dynamic properties of flow in regenerative cooled-nozzle. The computed results revealed thefollowing:

I. Nozzle with small radius of curvature ratio rc/rth of 0.625 internal flow calculation indicated radial flow deviations, the throat Mach number was 1.4 at the wall is found to be greater than the value of 0.8 at the axis.

II. For the same configuration (nozzle geometry and stagnation temperature), the wall heat transfer coefficient

increases with increasing Reynolds number due to higher mass flow. The inlet stagnation pressure can be changed to control the Reynolds number.

III. The main consequence of changing the stagnation temperature is to change the mass flux. At higher stagnation pressures, heat transfer coefficients are expected to decrease with increasing stagnation temperature, although this trend is less clear at low stagnation pressures.

IV. The wall static pressure increases as $\gamma$ decreases, while the separation flow location moves upstream with increasing specific heat ratio $\gamma$.

V. The boundary layer structure and the specified wall temperature affect the heat transfer distribution in the diverging region, right downstream of the adverse pressure gradient.

VI. Upstream of the throat, where the mass flux is maximum, the heat-transfer coefficient is largest.

VII. The rate of heat transfer, the wall static pressure, and the separation flow location are all affected by the wall temperature.

In general, the qualitative agreement was pretty good in all cases. The acquired results indicate a high level of consistency with the existing experimental data. The simulations provide information on heat transfer rate and separation flow for a variety of configurations, as well as answers questions about the impact of some parameters that aren't well discussed in the literature, such as the impact of wall temperature on separation position or the effect of stagnationtemperature on heat transfer rate.

## Nomenclature

| | | | |
|---|---|---|---|
| $a_1$ | Bradshow constant | $C_p$ | Specific heat at constant pressure |
| $E$ | Total energy | $C_v$ | Specific heat at constant pressure |
| $P$ | Pressure | $M$ | Mach number |
| $T$ | Temperature | $u_i$ | Mean velocities |
| $R$ | Gas constant | $p_{r_t}$ | Turbulent Prandtl number |
| $S$ | Scalar measure of strain tensor | $h$ | Heat transfer coefficient |
| $S_{ij}$ | strain tensor | $NPR$ | Chamber to ambient pressure |
| $\Omega$ | Scalar measure of vorticity tensor | $t$ | time |
| $\Omega_{ij}$ | vorticity tensor | $F_1, F_2$ | Auxiliary functions |
| $\bar{\Omega}_{ij}$ | Mean vorticity | $F$,$F_v$ | Convective, viscous flux vector |
| $k$ | Turbulence kinetic energy | | |
| $\omega$ | Specific dissipation rate [1/s] | Subscripts | |
| $x_i, x_j$ | Spatial coordinates | $aw$ | Adiabatic wall |
| $\rho$ | Density | $th$ | Throat position |
| $\gamma$ | Specific heat ratio | 0 | Nozzle entrance codition |
| $r$ | Radius, radial coordinate, recovery factor | $*$ | Initial point at the interaction region |
| $\mu_t$ | Turbulent eddy viscosity | $Sep$ | Separation position |
| $\mu$ | Dynamic viscosiy | $w$ | Wall position |

**Acknowledgements:** Present research has been carried out with the computational resource of CRIANN (Centre Régional Informatique et d'Applications Numériques de Normandie, Rouen, France)

## References

[1] Saunders, O.A. and Calder, P.H., Heat Transfer in a Nozzle at Supersonic Speeds. Proceedings of the Institution of Mechanical Engineers, Part B: Management and engineering manufacture, 1(1953), 1-12, pp. 232–239. https://doi.org/10.1177/002034835316701b16

[2] Ragsdale, W.C and Smith J.M, Heat transfer in nozzles," Chemical Engineering Science, 11(1959), 4, pp. 242–251, 0009-2509. https://doi.org/10.1016/S0009-2509(15)30003-8

[3] Baron, J.R. and Durgin, F.H., An experimental investigation of heat transfer at the boundaries of supersonic nozzles," WADC TR 54-541,1954, NavalSupersonic Laboratory, Mas- sachusetts institute of technology, WADC Technical Report 54-541.

[4] Kolozsi, J.J., An Investigation of Heat Transfer through the Turbulent Boundary Layer in an Axially Symmetric, Convergent-Divergent Nozzle," MS Thesis, Ohio State University, Columbus, OH, 1958.

[5] Back, L.H., Massier, P.F. and Gier, H.L., Convective Heat Transfer in a Convergent- Divergent Nozzle," Int. J. Heat Mass Transfer, 7(1964), pp. 549–568. https://doi.org/10.1016/0017-9310(64)90052-3

[6] Leccese, G., Bianchi, D., Betti, B., Lentini, D. and Nasuti, F., Convective and Radiative Wall Heat Transfer in Liquid Rocket Thrust Chambers, Journal of Propulsion and Power, 34(2018), 2, pp. 318–326. https://doi.org/10.2514/1.B36589.

[7] Arnold, R., Suslov, D. and Haidn O.J., Inuence Parameters on Film Cooling Effectiveness in a High Pressure Subscale Combustion Chamber, 47th AIAA Aerospace Sciences Meeting including The New Horizons Forum and Aerospace Exposition. Orlando, Florida, 2009. https://doi.org/10.2514/6.2009-453.

[8] Miranda, A. and Naraghi, M., Analysis of Film Cooling and Heat Trans- fer in Rocket Thrust Chamber and Nozzle," 49th AIAA Aerospace Sciences Meet- ing including the New Horizons Forum and Aerospace Exposition. Orlando, Florida, 2011. https://doi.org/10.2514/6.2011-712

[9] Kurtbas, I., The effect of different inlet conditions of air in a rectangular channel on convection heat transfer: Turbulence flow" Experimental Thermal and Fluid Science, 33(2008), I1, pp. 140-152, 0894-1777. https://doi.org/10.1016/j.expthermflusci.2008.07.012

[10] Betti, B., Bianchi, D., Nasuti, F. and Martelli, E., Chemical Reaction Effects on Wall Heat Flux in Liquid Rocket Thrust Chambers, 50th AIAA/ASME/SAE/ASEE Joint Propulsion Conference Cleveland, OH, 2014. https://doi.org/10.2514/6.2014-3675

[11] Kim, J.G., Lee, J.W. and Kim, K.H., Investigation on the Characteristics of Plume- Induced Flow Separation and Wall Heat Transfer, Journal of Spacecraft and Rockets, 49(2012), 1, pp. 189–192. https://doi.org/10.2514/1.51782

[12] Daimon, Y., Negishi, H., Yamanishi, N., Nunome, Y., Sasaki, M. and Tomita, T., Combustion and Heat Transfer Modeling in Regeneratively Cooled Thrust Chambers (Optimal Solution Procedures for Heat Flux Estimation of a Full-Scale Thrust Chamber), 48th AIAA/ASME/SAE/ASEE Joint Propulsion Conference and Exhibit, Joint Propulsion Conferences, 2012. DOI:10.2514/6.2012-4009.

[13] Frank, G. and Pfitzner, M., Investigation of the heat transfer coefficient in a tran- spiration film cooling with chemical reactions, International Journal of Heat and Mass Transfer, 113(2017), pp. 755-763, 0017-9310. https://doi.org/10.1016/j.ijheatmasstransfer.2017.05.103

[14] Xiao, X., Hassan, H.A. and Edwards, J.R., Role of Turbulent Prandtl Numbers on Heat flux at Hypersonic Mach Numbers, AIAA, 45(2007), 4, pp. 806–813. https://doi.org/10.2514/1.21447

[15] Sommer, T.P., So, R.M.C. and Zhang, H.S., A Near Wall Variable Turbulent- Prandtl-Number Turbulence Model For Compressible Flows, AIAA, 31(1993), 1, pp. 27-35. https://doi.org/10.2514/3.11314.

[16] Vieser, W., Esch, T. and Menter, F., Heat Transfer Predictions Using Advanced Two-Equation Turbulence Models, CFX/ANSYS, Tech. Rept. CFX-VAL 10/0602, Otterfing, Germany, 2002.

[17] Tong, X.L, Luke, E., Turbulence Models and Heat Transfer in Nozzle Flows, AIAA, 42(2004), 11, pp. 2391-2393. https://doi.org/10.2514/1.8900

[18] MacCormack, R.W., Current status of numerical solution of the Navier-Stokes equations, AIAA, 2012. https://doi.org/10.2514/6.1985-32.

[19] J. Steger and R.F. Warming, Flux vector splitting of the invisid gas dynamics equations with application to finite difference methods, NASA, TM-78605, 1979. https://doi.org/10.1016/0021-9991(81)90210-2.

[20] Campbell, C. and Farley, J., Performance of several conical convergent-divergent rocket type exhaust nozzles, NASA , TN D-467, 1960.

[21] Bensayah, K., Kamri, K., Numerical investigation of supersonic flow separation in thrust-optimized contour rocket nozzle, Journal of the Serbian Society for Computational Mechanics, 16(2022), 2, pp. 43-55. 10.24874/jsscm.2022.16.02.03.

[22] Bensayah, K, Hadjadj, A. and Bounif, A., Heat Transfer in Turbu- lent Boundary Layers of Conical and Bell Shaped Rocket Nozzles with Com- plex Wall Temperature," Numerical Heat Transfer part-a, 66(2014),pp. 289–314. http://dx.doi.org/10.1080/10407782.2013.873283.
[23] Bensayah, K, Mahfoudi, El., Numerical prediction of compressible heat flow with complex wall temperature in supersonic rocket nozzles" Thermal Science, 22(2018),6 part B, pp. 3043–3056. https://doi.org/10.2298/TSCI160616270B.
[24] Délery, J. and Marvin, J., Shock-Wave boundary layer Interactions, volume AGAR-Dograph N. 28, AGARD, 1986.
[25] Schmucker, R.H., Status of flow separation prediction in liquid propellant rocket nozzles, Technical Memorandum TM X-64890. NASA, George C. Marshall Space Flight Center, 1974.
[26] Lebedev, V.P., Lemanov, V.V. and Terekhov, V.I., 2006, Film-Cooling Efficiency in a Laval Nozzle Under Conditions of High Freestream Turbulence, Journal of Heat Transfer, 128(2006), pp. 571-579. https://doi.org/10.1115/1.2188508
[27] Sommer, T.P., So, R.M.C. and Zhang, H.S., A Near Wall Four-Equation Turbulence model for Compressible Boundary Layers, NASA Contractor Report (NASA-CR-4436), Arizona State Univ, 1994.
[28] Ljuboja, M. and Rodi, W., Prediction of Horizontal and Vertical Turbulent Buoyant Wall Jets., J. Heat Transfer, 103(1981),2, pp. 343–349. https://doi.org/10.1115/1.3244464.
[29] Cuffel, R.F., Back, L.H. and Massier, P.F., Transonic Flow field in a Supersonic Nozzle with Small Throat Radius of Curvature, AIAA Paper, 7(2012), 7, pp. 1364-1366

Paper submitted: 13 May 2023
Paper revised: 30 July 2023
Paper accepted: 05 August 2023